PROCEEDINGS OF THE 8TH INTERNATIONAL CONFERENCE ON DISCRETE ELEMENT METHODS
(DEM8)

DYNAMICS OF DISCRETE WET GRANULAR AVALANCHES IN A ROTARY DRUM

Jens H. Kasper[1], **Vanessa Magnanimo**[1] **and Ahmed Jarray**[1]

[1] Multi Scale Mechanics (MSM), University of Twente.
NL-7500 AE Enschede, The Netherlands.
j.h.kasper@student.utwente.nl

Keywords Granular Materials, Granular Avalanche, Liquid Induced Cohesion, Rotary Drum, DEM.

Abstract The dynamic behavior of cohesive granular flows is important in geo-mechanics and industrial applications, yet poorly understood. We studied the effects of liquid viscosity and particle size on the dynamics of wet granular avalanches, occurring in a slowly rotating drum. A Discrete Element Method (DEM) model, in which contact forces and cohesive forces were considered, was employed to simulate this flow behavior. We found that the avalanche amplitude, flow layer velocity and granular temperature decrease as viscosity increases, but increase with particle size. Increasing the viscous forces causes the flow to behave as a bulk, pushing the free surface towards a convex shape, and avalanches become less pronounced. We found that this transition from avalanching flow to continuous flow can be characterized by evaluating the local fluctuations of the surface angle.

1 INTRODUCTION

Granular flows have been extensively studied by physicists over the past years [1]. Understanding the dynamics of flowing granular matter is important in both industrial applications and the management of geo-physical problems, such as landslides and avalanches. A granular avalanche occurs when the slope of a pile of grains exceeds its maximum angle of stability θ_m, whereafter the surface angle decreases until the angle of repose θ_r is reached. Rotary drums filled with particles are practical geometries which have been adopted extensively to mimic granular avalanches and to study their flow properties [3–10]. At a low rotational speed, avalanches occur periodically, while at high rotational speeds a continuous flow is observed.

Avalanche dynamics can be characterized by the evolution of the slope angle and particle velocity. The avalanche amplitude $\Delta\theta = \theta_m - \theta_r$ is found to be of well defined, finite value [2], and is observed to increase with particle size [4]. The velocity profile during an avalanche shows an exponentially decreasing trend in pile depth direction (perpendicular to the pile surface) and no steady state is observed during the avalanche [5]. The variance

of the particle velocity $\delta v^2 = \langle v^2 \rangle - \langle v \rangle^2$ remains equal to zero when the particles are at rest with respect to the drum [6]. As an avalanche occurs, δv^2 peaks shortly before gradually decreasing.

By wetting the particles, capillary bridges are formed between them, which induce cohesive forces and alter pile stability and the flow properties of avalanches [7, 11]. Wet granular avalanches have not been researched as much as dry avalanches and show qualitatively new behaviour [8]. Several regimes have been identified, characterizing flow behavior, based on liquid volume [7], and liquid density and viscosity [8]. However, the dynamics of wet granular avalanches remain poorly understood and relations between several microscopic and macroscopic parameters are lacking.

The work presented here focuses on understanding the effects of the viscosity of the interstitial liquid and the particle size on wet granular avalanches. We used a Discrete Element Method (DEM) model to simulate avalanches and we examined the evolution of the slope angle, particle velocity and velocity fluctuations (granular temperature). The obtained results have important implications for geo-mechanics and landslide control.

2 NUMERICAL MODELING

The software package LIGGGHTS [12] was used to simulate wetted particles in a rotary drum, using the Discrete Element Method. Particle trajectories are calculated by solving Newton's equations of motion, in which we considered contact forces and cohesive forces. The movement of an arbitrary particle i, which is in contact with a set of $j = 1, ..., k$ adjacent particles, is described by [13]:

$$m_i \ddot{\mathbf{x}}_i = \sum_{j=1}^{k} (\mathbf{F}_{ij}^c + \mathbf{F}_{ij}^l) + m_i \mathbf{g}, \tag{1}$$

$$I_i \ddot{\boldsymbol{\theta}}_i = \sum_{j=1}^{k} (\mathbf{h}_{ij} \times (\mathbf{F}_{ij}^c + \mathbf{F}_{ij}^l) + \mathbf{q}_{ij}), \tag{2}$$

with mass m_i, position $\mathbf{x}_i$, contact force $\mathbf{F}_{ij}^c$, cohesive force $\mathbf{F}_{ij}^l$, gravity $\mathbf{g}$, mass moment of inertia I_i, angular position $\boldsymbol{\theta}_i$, distance-to-contact point vector $\mathbf{h}_{ij}$ and additional torque $\mathbf{q}_{ij}$ (due to rolling). Note that variables printed in bold represent vectors.

2.1 Contact model

A linear spring-dashpot model [12,14,15] was used to compute the total frictional force $\mathbf{F}_{ij}^c$ between two colliding particles i and j. $\mathbf{F}_{ij}^c$ is nonzero only if there is a positive absolute normal overlap δ_n between the particles, which is defined as:

$$\delta_n = (r_i + r_j) - (\mathbf{x}_i - \mathbf{x}_j) \cdot \mathbf{n}_{ij}, \tag{3}$$

where r is the particle radius. When $\delta_n > 0$, $\mathbf{F}_{ij}^c$ is computed as:

$$\mathbf{F}_{ij}^{c} = (k_n \boldsymbol{\delta}_n + \gamma_n \dot{\boldsymbol{\delta}}_n) + (k_t \boldsymbol{\delta}_t + \gamma_t \dot{\boldsymbol{\delta}}_t), \tag{4}$$

with elastic constant k, overlap $\boldsymbol{\delta}$ and visco-elastic damping constant γ. The subscripts n and t denote normal and tangential directions respectively. Furthermore, $\boldsymbol{\delta}_t$ is truncated to fulfill:

$$\left|(k_t \boldsymbol{\delta}_t + \gamma_t \dot{\boldsymbol{\delta}}_t)\right| \leq \mu_F \left|(k_n \boldsymbol{\delta}_n + \gamma_n \dot{\boldsymbol{\delta}}_n)\right|, \tag{5}$$

with coefficient of friction (CoF) μ_F, to ensure the satisfaction of Coulomb′s law of attrition. The Hertz-Mindlin model [12, 16], based on Hertz theory in normal direction and the Mindlin no-slip improved model in tangential direction, was employed to calculate the elastic and damping constants. k_n is calculated using:

$$k_n = \frac{4}{3}\left(\frac{1-\nu_i^2}{E_i} + \frac{1-\nu_j^2}{E_j}\right)^{-1} \sqrt{R^* \delta_n}, \tag{6}$$

with modulus of elasticity E, Poisson′s ratio ν and effective radius R^*. γ_n is computed as:

$$\gamma_n = -\frac{2\sqrt{15}}{3} \frac{\ln(e)}{\sqrt{\ln^2(e) + \pi^2}} \sqrt{\left(\frac{1}{\rho_1 \pi r_i^3} + \frac{1}{\rho_2 \pi r_j^3}\right)^{-1} k_n}, \tag{7}$$

with coefficient of restitution (CoR) e and particle density ρ. As for the tangential components, k_t is defined as:

$$k_t = 8\left(\frac{2-\nu_i}{G_i} + \frac{2-\nu_j}{G_j}\right)^{-1} \sqrt{R^* \delta_n}, \tag{8}$$

with shear modulus G and γ_t is defined as:

$$\gamma_t = -\frac{2\sqrt{10}}{3} \frac{\ln(e)}{\sqrt{\ln^2(e) + \pi^2}} \sqrt{\left(\frac{1}{\rho_1 \pi r_i^3} + \frac{1}{\rho_2 \pi r_j^3}\right)^{-1} k_t}. \tag{9}$$

A constant directional torque model [12,17] was implemented to account for rolling resistance, by contribution of additional torque vector $\mathbf{q}_{ij}$, given by:

$$\mathbf{q}_{ij} = \mu_{RF} k_n \delta_n R^* \frac{(\dot{\boldsymbol{\theta}}_i - \dot{\boldsymbol{\theta}}_j)}{\left|(\dot{\boldsymbol{\theta}}_i - \dot{\boldsymbol{\theta}}_j)\right|}, \tag{10}$$

with coefficient of rolling friction (CoRF) μ_{RF}. In the case of particle-wall contact, equations (6-10) are taken in the limit of particle j going to infinite radius.

2.2 Liquid cohesion model

A composition of models, as suggested by Easo et al. [12, 18], was used to define the cohesive force between particles i and j. It is assumed that a surface liquid film exists on each particle, allowing for a liquid bridge to form upon contact with another particle. For the purpose of the cohesion model, particles are considered to be in contact only if δ_n satisfies:

$$-0.1(r_i + r_j) \leq \delta_n \leq -0.01(r_i + r_j). \tag{11}$$

The bridge ruptures when $|\mathbf{x}_i - \mathbf{x}_j|$ exceeds the rupture distance d_0, which is given by [19]:

$$d_0 = (\frac{1}{2} + \frac{(\alpha_i + \alpha_j)}{4})V_{bond}^{1/3}, \tag{12}$$

with contact angle α and liquid bond volume V_{bond}. It is assumed that V_{bond} is 5% of the combined liquid film volume, and that distributes evenly over the two particles after bridge rupture. The total cohesive force $\mathbf{F}_{ij}^l$ between the particles is defined as:

$$\mathbf{F}_{ij}^l = \mathbf{F}_{cap} + \mathbf{F}_{vis}, \tag{13}$$

with capillary force $\mathbf{F}_{cap}$ and viscous force $\mathbf{F}_{vis}$. The capillary force acts in normal direction and is defined by Soulie et al. [20] as:

$$\mathbf{F}_{cap} = \pi\sigma\sqrt{r_i r_j}(c + \exp(a\frac{-\delta_n}{r_{max}} + b))\mathbf{n}, \tag{14}$$

with liquid surface tension σ and r_{max} being the larger of r_i and r_j. Variables a, b and c are given by:

$$a = -1.1(\frac{V_{bond}}{r_{max}^3})^{-0.53}, \tag{15}$$

$$b = (-0.037\ln(\frac{V_{bond}}{r_{max}^3}) - 0.24)(\alpha_i + \alpha_j)^2 - 0.0082\ln(\frac{V_{bond}}{r_{max}^3}) + 0.48, \tag{16}$$

$$c = 0.0018\ln(\frac{V_{bond}}{r_{max}^3}) + 0.078. \tag{17}$$

The viscous force consists of a normal and tangential component and is described by Nase et al. [21] as:

$$\mathbf{F}_{vis} = 6\pi\mu R^*(\frac{R^*}{-\delta_n}\dot{\boldsymbol{\delta}}_n + (\frac{8}{15}\ln(\frac{R^*}{-\delta_n}) + 0.9588)\dot{\boldsymbol{\delta}}_t), \tag{18}$$

with liquid viscosity μ. In the case of particle-wall contact, $\mathbf{F}_{cap}$ and $\mathbf{F}_{vis}$ are equal to zero.

2.3 Simulation parameters

The particles and drum were given the properties that are summarised in Tables 1 and 2, which respectively mimic glass [22] and wood [23] material properties. In all simulations, the drum was filled for 35% with a mono-disperse set of particles and rotated at a constant rotational speed Ω of 0.5 rpm. The particles had a radius r of either 1.25mm, 2mm or 3mm.

Table 1: Particle parameters.

Parameter	**Value**
Radius, r [mm]	1.25, 2.0, 3.0
Density, ρ [kg/m^3]	2500
Young$'s$ mod., E [MPa]	63
Poisson$'$s ratio, ν [-]	0.21
CoR, e^{pp} [-]	0.95
CoF, μ_F^{pp} [-]	0.10 (wet)
	0.40 (dry)
CoRF, μ_{RF}^{pp} [-]	0.01

Table 2: Drum parameters.

Parameter	**Value**
Radius, R [m]	0.0605
Width, w [m]	0.022
Young$'s$ mod., E [MPa]	12
Poisson$'$s ratio, ν [-]	0.35
CoR, e^{wp} [-]	0.72
CoF, μ_F^{wp} [-]	0.15 (wet)
	0.30 (dry)
CoRF, μ_{RF}^{wp} [-]	0.01

Dry simulations were performed, as well as simulations in which 4 cm^3 of interstitial liquid was included. The simulated liquids were modeled to mimic water-glycerol mixtures [24], with glycerol concentration ϕ varying from 0% to 100%. The surface tension σ and contact angle α of water (σ = 72 mN/m, $\alpha = 35°$) and glycerol (σ = 62 mN/m, $\alpha = 38°$) are nearly the same, while their viscosity strongly varies. This makes water-glycerol mixtures exceptionally suitable for studying the influence of liquid viscosity on the avalanche dynamics. We used seven distinct mixtures in total, with properties as given in Table 3. Dry simulations are assigned case number $n = 0$.

Table 3: Liquid mixture parameters.

Parameter	**Value**						
Case number, n	1	2	3	4	5	6	7
Concentration glycerol, ϕ [%]	0	85	91	93	95	98	100
Viscosity, μ [mPa·s]	1.01	109	219	367	523	939	1410

In each simulation, the particle positions and velocities were tracked for 50 seconds, allowing the examination of the surface angle and velocity profiles. The software package ParaView [25] and several filters in python were used to evaluate the surface angle θ, the avalanche amplitude $\Delta\theta = \theta_m - \theta_r$ and the translational granular temperature T_g. In

the evaluation of $\Delta\theta$, a threshold was used to filter out some of the smaller fluctuations caused by noise. T_g was defined as:

$$T_g = \frac{1}{3}\Big(< U_x^2 > + < U_y^2 > + < U_z^2 > \Big), \tag{19}$$

with fluctuation velocity U_i, given by:

$$U_i = u_i - < u_i >, \quad i = x, y, z, \tag{20}$$

which was evaluated locally to always include circa 7 surrounding particles. The velocity profiles were obtained using a Gaussian Kernel point volume interpolation scheme.

3 RESULTS AND DISCUSSION

Figure 1(a) shows a typical evolution of the surface angle during several successive dry avalanches. Maximum stability and repose angles θ_m and θ_r, show as respectively the local maxima and minima in the "sawtooth"-like curve. The avalanches are very pronounced; particles are periodically at rest with respect to the drum and flowing down in a surface layer [Figure 2(a)]. This is further illustrated by the evolution of the granular temperature T_g, shown in Figure 1(b). The peaks observed during the avalanches indicate large relative movements between particles, while in between avalanches, T_g drops to near zero. Qualitatively similar behavior is observed for wet granular avalanches with an interstitial liquid of low viscosity ($\mu = 1.01$ mPa·s, $n = 1$), shown in Figures 1(c)-(d) by the continuous blue line. However, for a high viscosity case ($\mu = 1410$ mPa·s, $n = 7$), the evolution of the surface angle does not show a periodically steady trend. Smaller fluctuations occur more frequently, while distinct avalanches do not occur at all, implying a more continuous flow. The development of T_g seems to support this theory, as the peaks, for decreasing θ, are significantly smaller. Furthermore, when θ is increasing, T_g does not drop to zero, indicating that particles are never all at rest with respect to the drum.

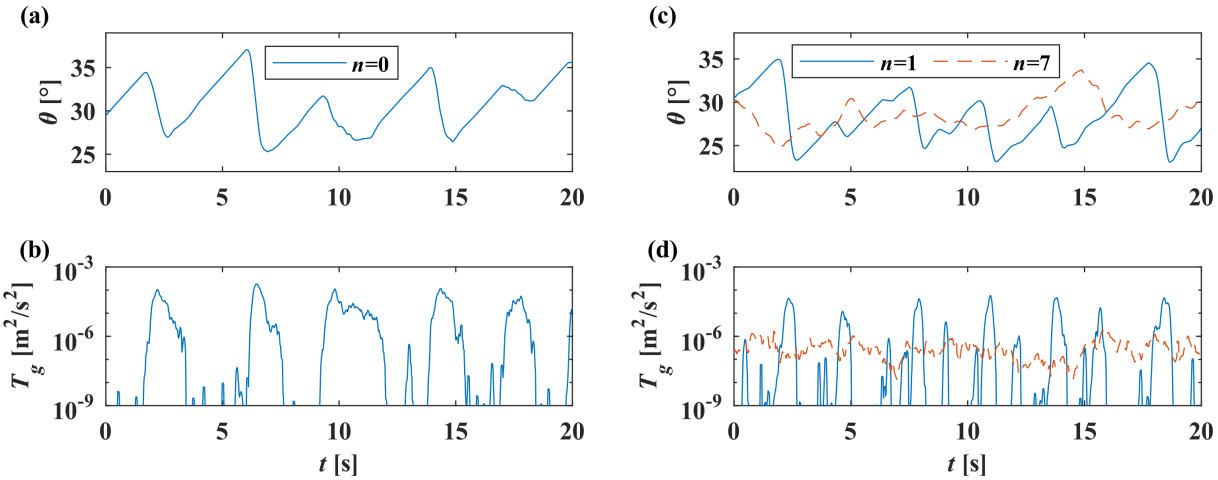

Figure 1: Time evolution of granular avalanches with particles of $r = 2$mm. (a) θ and (b) T_g for the dry case $n = 0$. (c) θ and (d) T_g for the low viscosity wet case $n = 1$ and high viscosity wet case $n = 7$.

An interesting feature of the avalanches shown in Figures 1(a) and 1(b) is the rather large variation in amplitude $\Delta\theta$ of successive avalanches. A slower rotational speed of the drum Ω is likely to reduce these variations and provide an even more periodic trend [3, 4].

Figures 2(a)-(d) show typical velocity profiles for avalanches with low to high fluid viscosity. In all cases, a high velocity flow layer near the surface is observed, while below this layer particles are at rest with respect to the drum and move only due to its rotational speed. The dry case $n = 0$ yields a larger flow layer velocity v than the wet cases, for which v decreases as viscosity increases. This result has also been observed by Brewster et al. [28], who found that cohesive forces limit the development of the velocity in the flow layer. Figure 2(e) shows the particle velocity along the diagonal d, normal to the free flowing surface (pile height direction, starting from the border of the drum). In all cases, the velocity of the flow layer increases linearly initially, before leveling out slightly. The steepness of the velocity curve, decreases with the viscosity, and is the highest for the dry case. However, the thickness of the flow layer appears to be independent of fluid viscosity.

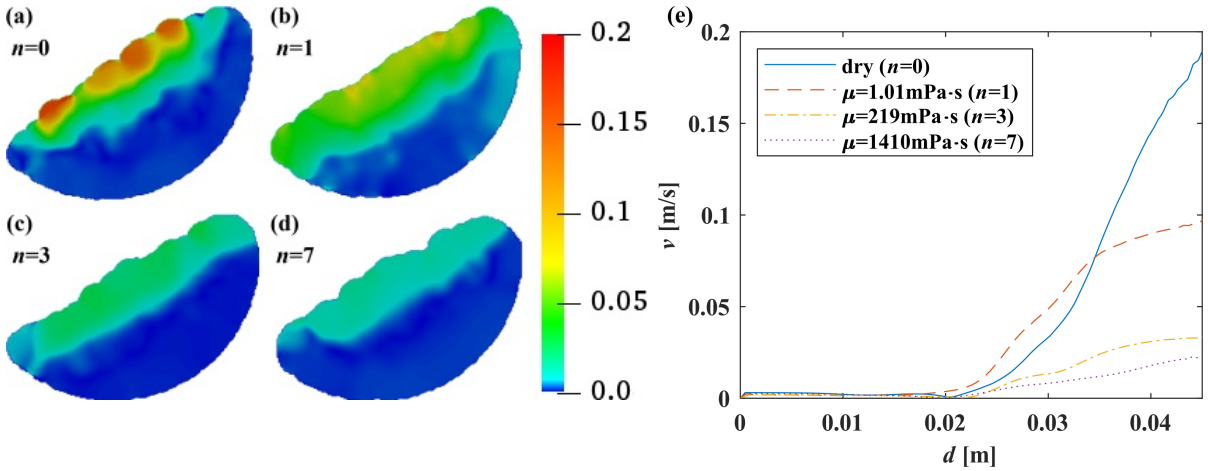

Figure 2: Velocity profiles during granular avalanches with particles of $r = 2$mm. (a) the dry case $n = 0$. (b), (c) and (d) the wet cases $n = 1, 3, 7$ respectively, with viscosities of $\mu = 1.01$mPa·s, $\mu = 219$mPa·s and $\mu = 1410$mPa·s. (e) particle velocity as a function of pile height d for $n = 0, 1, 3, 7$.

Simulations with particles of $r = 1.25$mm and $r = 3$mm show qualitatively similar behavior to those with $r = 2$mm shown in Figures 1 and 2. The flow layer velocity was observed to increase in magnitude with particle size, yet the overall trends remained alike. Figures 3(a)-(b) show the time averaged avalanche amplitude $< \Delta\theta >$ and granular temperature $< T_g >$ respectively, as function of liquid viscosity, for several particle sizes. Note that as μ increases, $< \Delta\theta >$ becomes less a measure of avalanche amplitude, and more a measure of surface angle fluctuation in time, as the flow transitions away from the avalanching regime. For all particle sizes, $< \Delta\theta >$ and $< T_g >$ are observed to decrease exponentially with increasing viscosity and saturate at high values of μ, agreeing with

statements by Courrech du Pont et al. [7]. For the dry case, the granular temperature $< T_g >$ is of an order of magnitude greater than for the viscous cases. It appears that the liquid induced cohesive bonds between particles tend to reduce relative particle motion, causing particles to clump together, which reduces the number of inter-particles collisions. This effect gets magnified as liquid viscosity increases and the cohesive bonds become stronger.

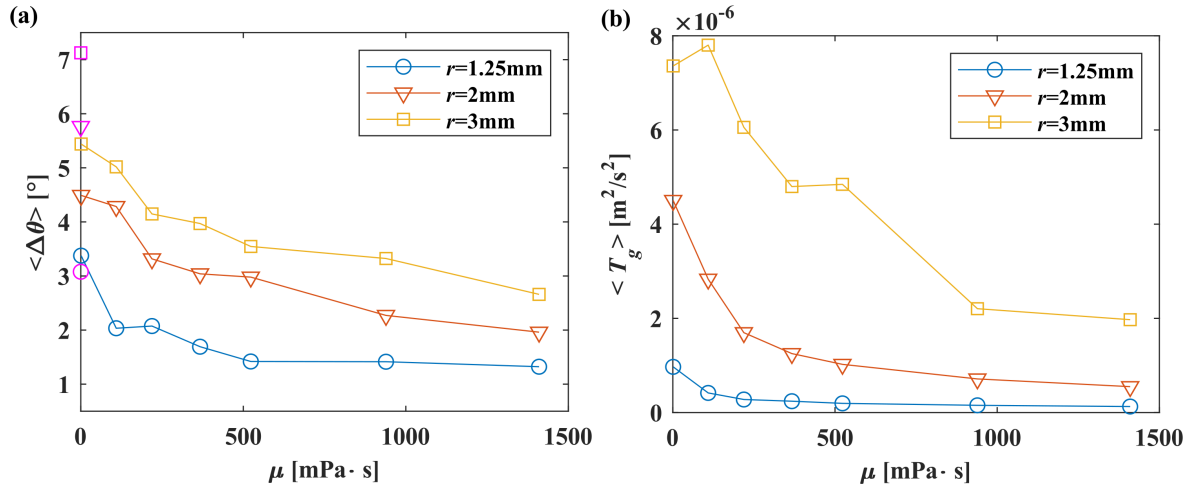

Figure 3: Time averaged flow properties as function of liquid viscosity, for several particle sizes. (a) $< \Delta\theta >$ and (b) $< T_g >$. Symbols colored in magenta represent simulations with dry conditions.

The avalanche amplitude is shown to increase with r in Figure 3(a). This trend is consistent with experimental research on dry [4] and wet [7] granular avalanches, in which larger avalanches are observed as the particle over drum radius ratio $\frac{r}{R}$ increases. The granular temperature is shown to increase with particle size as well. As $\frac{r}{R}$ increases, $< T_g >$ is evaluated over a larger local volume and thus larger relative movements are indeed expected. Interestingly, the curves for $r = 1.25$mm and $r = 2$mm are quite smooth, while for $r = 3$mm some outliers appear. This is likely due to interlocking of particles, caused by the low drum over particle size ratio ($\frac{R}{r} \approx 20$).

Figure 4(a) shows the time averaged surface angle $< \theta >$, with standard deviations, as function of μ, for several particle radii. For the dry case, $< \theta >$ increases with particle size, in agreement with observations by various authors [3, 4]. For the wet cases, $< \theta >$ shows a vague but decreasing trend for increasing r, which agrees with observations made by Nowak et al. [27]. Again, some outlying points appear for simulations with particles of $r = 3$mm, possibly the result of interlocking. The average angle does not seem to depend on μ in any significant manner.

The evolution of the avalanche amplitude $\Delta\theta$ and granular temperature T_g, presented in Figures 1 and 3, indicate that the granular flow transitions from an avalanching flow towards a continuous flow as viscosity increases. For granular flows in the avalanching

regime, the surface angle is in general observed to be constant along the surface [2, 3]. For continuous flows, the surface is observed to be "S-shaped" if cohesion is low and $\Omega > 5$rpm [26], or even slightly convex if cohesive forces are large [28]. It appears that local fluctuations in the surface angle (i.e. the deviation between the local surface angle and the average angle of the whole surface) indicate a measure of "continuousness" in the granular flow. We approximate which particles make up the surface layer by dividing the drum into N bins and considering the top particle in each bin. Polyfitting a linear function through the coordinates of all surface particles yields a flat averaged surface. The local fluctuations in surface angle are evaluated by measuring the average absolute deviation Δh, of the distance between the surface particles and the polyfitted surface. Δh is thus defined as:

$$\Delta h = \frac{1}{N}\sum_{i=1}^{N}\sqrt{(x_i - x_i^{fit})^2 + (y_i - y_i^{fit})^2}, \tag{21}$$

in which (x_i, y_i) denote particle coordinates and (x_i^{fit}, y_i^{fit}) denote points on the polyfitted surface. Figure 4(b) shows that indeed $< \Delta h >$ increases with liquid viscosity, while $< \Delta\theta >$ decreases. We can infer that the value of μ at which the transition from an avalanching to a continuous flow happens, is around the intersection point between the averaged avalanche amplitude and the local angle fluctuation.

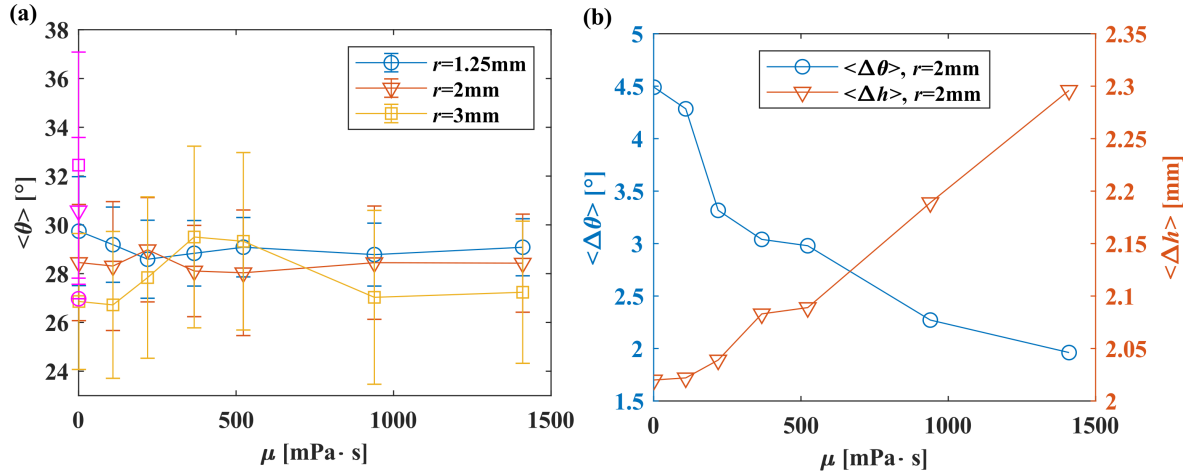

Figure 4: (a) $< \theta >$ as function of liquid viscosity, for several particle sizes. Symbols colored in magenta represent simulations with dry conditions. (b) $< \Delta\theta >$ and $< \Delta h >$, for simulations with particles of $r = 2$mm only.

4 CONCLUSION

Using Discrete Element Method simulations, we have investigated how the dynamics of wet granular avalanches in a rotary drum are affected by the viscosity of the interstitial

liquid and the particle size. Discrete avalanches were observed for the dry case and the wet cases with relatively low viscosity. As viscosity increases, the flow transitions from the avalanching regime to the rolling regime, which is characterized by a more continuous flow. This transition is indicated by a decrease in avalanche amplitude, flow layer velocity and granular temperature, and an increase in local fluctuations of the surface angle. Increasing the viscous forces causes the flow to behave as a bulk, pushing the free surface towards a convex shape.

As the particle size increases, the avalanche amplitude, flow layer velocity and granular temperature increase as well, indicating an increase in relative importance of inertial effects with respect to frictional forces and viscous forces.

The results suggest that the effects of liquid viscosity and particle size should be considered when studying granular avalanches, whether for large scale investigation, pilot scale experiments or for further numerical simulations.

REFERENCES

[1] Duran J. (2000). *Sands, Powders, and Grains*. New York: Springer.

[2] Jaeger, H.M., Liu, C.H. and Nagel, S.R. (1989). Relaxation at the angle of repose. *Physical Review Letters* 62, 40–43.

[3] Fischer, R., Gondret, P., Perrin, B. and Rabaud, M. (2008). Dynamics of dry granular avalanches. *Physical Review E - Statistical, Nonlinear, and Soft Matter Physics* 78(2), 021302.

[4] Balmforth, N.J. and McElwaine, J.N. (2018). From episodic avalanching to continuous flow in a granular drum. *Granular matter* 20(3), 52.

[5] Courrech du Pont, S., Fischer, R., Gondret, P., Perrin, B. and Rabaud, M. (2005). Instantaneous velocity profiles during granular avalanches. *Physical Review Letters* 94(4), 048003.

[6] Li, R., Yang, H., Zheng, G. and Sun, Q.C. (2018). Granular avalanches in slumping regime in a 2D rotating drum. *Powder Technology* 326, 322–326.

[7] Courrech du Pont, S., Gondret, P., Perrin, B. and Rabaud, M. (2003). Granular avalanches in fluids. *Physical Review Letters* 90(4), 443011–443014.

[8] Tegzes, P., Vicsek, T. and Schiffer, P. (2002). Avalanche Dynamics in Wet Granular Materials. *AIP Conference Proceedings* 89(9), 094301.

[9] Liu, P.Y., Yang, R.Y. and Yu, A.B. (2013). Particle scale investigation of flow and mixing of wet particles in rotating drums. *AIP Conference Proceedings* 1542, 963–966.

[10] Jarray, A., Magnanimo, V. and Luding, S. (2017). Scaling of wet granular flows in a rotating drum. *EPJ Web of Conferences* 140, 03078.

[11] Hornbaker, D.J., Albert, R., Albert, I., Barabasi, A. and Schiffer, P. (1997). What keeps sandcastles standing? *Nature* 387(6635), 765.

[12] Kloss, C., Goniva, C., Hager, A., Amberger, S. and Pirker, S. (2012). Models, algorithms and validation for opensource DEM and CFD-DEM *Progress in Computational Fluid Dynamics, An International Journal* 12(2–3), 140–152.

[13] Luding, S. (2008). Introduction to Discrete Element Methods: Basics of Contact Force Models. *European journal of environmental and civil engineering* 12(7–8), 785–826.

[14] Di Renzo, A. and Di Maio, F.P. (2005). An improved integral non-linear model for the contact of particles in distinct element simulations. *Chemical Engineering Science* 60, 1303–1312.

[15] Silbert, L.E., Erta, D., Grest, G.S., Halsey, T.C., Levine, D. and Plimpton, S.J. (2001). Granular flow down an inclined plane: Bagnold scaling and rheology. *Physical Review E - Statistical, Nonlinear, and Soft Matter Physics* 64(5), 1–14.

[16] Mindlin, R.D. and Deresiewicz, H. (1953). Elastic Spheres in Contact under Varying Oblique Forces. *Journal of applied mechanics* 20, 327–344.

[17] Ai, J., Chen, J.F., Rotter, J.M. and Ooi, J.Y. (2011). Assessment of rolling resistance models in discrete element simulations. *Powder Technology* 206(3), 269–282.

[18] Easo, L.A. and Wassgren, C.R. (2013). Comparison of Liquid Bridge Volume Models in DEM Simulations. *2013 AIChE Annual Meeting* 1, 159b.

[19] Lian, G., Thornton, C. and Adams, M.J. (1993). A Theoretical Study of the Liquid Bridge Forces between Two Rigid Spherical Bodies. *Journal of Colloid and Interface Science* 161, 138–147.

[20] Soulie, F., Cherblanc, F., El Youssoufi, M.S. and Saix, C. (2005). Influence of liquid bridges on the mechanical behaviour of polydisperse granular materials. *International Journal for Numerical and Analytical Methods in Geomechanics* 30(3), 213–228.

[21] Nase, S. T., Vargas, W. L., Abatan, A.A. and McCarthy, J.J. (2001). Discrete characterization tools for cohesive granular material. *Powder Technology* 116(2), 214–223.

[22] Sigmund Lindner (2015). *SiLibeads Glass beads Type S, Microglass beads: Product Data Sheet.* Warmensteinach: Sigmund Lindner.

[23] Granta Design (2017). *CES EduPack 2017.* Cambridge: Granta Design.

[24] Glycerine Producers Association (1963). *Physical Properties of Glycerine and Its Solutions.* New York: Glycerine Producers Association.

[25] Ayachit U. (2016). *The ParaView Guide: A Parallel Visualization Application.* New York: Kitware.

[26] Jarray, A., Magnanimo, V. and Luding, S. (2019). Wet granular flow control through liquid induced cohesion. *Powder technology* 341, 126–139.

[27] Nowak, S., Samadani, A. and Kudrolli, A. (2005). Maximum angle of stability of a wet granular pile. *Nature Physics* 1, 50–52.

[28] Brewster, R., Grest, G.S. and Levine, A.J. (2009). Effects of cohesion on the surface angle and velocity profiles of granular material in a rotating drum. *Physical Review E* 79, 011305.